^{14}N nuclear quadrupole coupling and methyl internal rotation in the microwave spectrum of 2-methylpyrrole

Thuy Nguyen,[a] Christina Dindic,[b] Wolfgang Stahl,[b] Ha Vinh Lam Nguyen,[a*] and Isabelle Kleiner[a]

[a] *Laboratoire Interuniversitaire des Systèmes Atmosphériques (LISA), CNRS UMR 7583, Université Paris-Est Créteil, Université de Paris, Institut Pierre Simon Laplace (IPSL), 61 avenue du Générale de Gaulle, F-94010 Créteil, France*

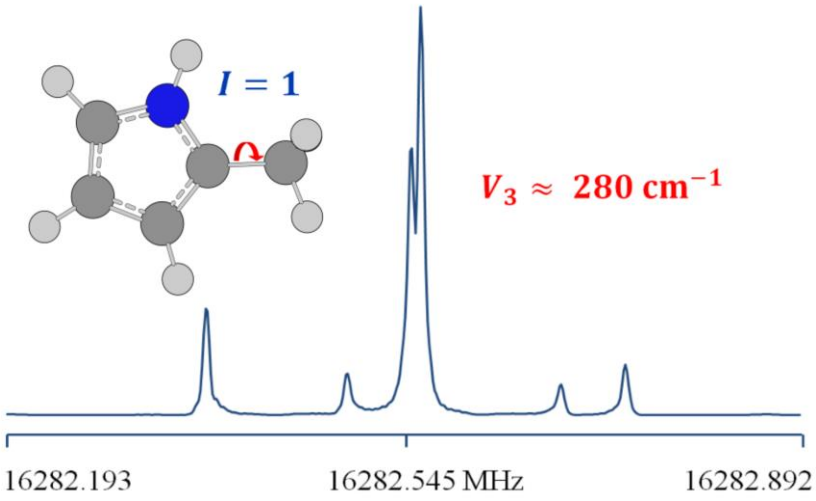
[b] *Institute of Physical Chemistry, RWTH Aachen University, Landoltweg 2, D-52074 Aachen, Germany*

*Corresponding author: Ha Vinh Lam Nguyen
Laboratoire Interuniversitaire des Systèmes Atmosphériques (LISA), UMR CNRS 7583, Université Paris-Est-Créteil, Université de Paris, Institut Pierre Simon Laplace (IPSL), Créteil, France
Phone: 0033 1 82 39 20 44
Email: lam.nguyen@lisa.u-pec.fr

^{14}N nuclear quadrupole coupling and methyl internal rotation in the microwave spectrum of 2-methylpyrrole

Using two molecular jet Fourier transform microwave spectrometers, the rotational spectrum of 2-methylpyrrole was recorded in the frequency range from 2 to 40 GHz. From the torsional splittings due to the internal rotation of the methyl group a barrier height of 279.7183(26) cm^{-1} was deduced. Because of the ^{14}N nucleus, all lines show a quadrupole hyperfine structure. The microwave spectra were analyzed using the *XIAM* and *BELGI-C_s-hyperfine* codes. The *XIAM* code enabled us to reproduce the whole data set with a root-mean-square deviation of 5.6 kHz while the *BELGI-C_s-hyperfine* code could provide a better root-mean-square almost by a factor of 2 compared to that of *XIAM*. The experimental results were complemented by quantum chemical calculations. The values of the methyl torsional barrier and the ^{14}N nuclear quadrupole coupling constants are discussed and compared with other methyl substituted pyrroles as well as other aromatic five-membered rings.

Keywords: 2-methylpyrrole, microwave spectrum, internal rotation, nuclear hyperfine.



Introduction

For many years, the phenomenon of internal rotation has been a subject of considerable interest to both chemists and physicists. Studies of potential functions, barrier heights, stability of rotational isomers, and ring conformations provide basic information for testing and improving methods to understand the effects of internal rotation. Quantum chemical calculations together with molecular jet Fourier transform microwave (MJ-FTMW) spectroscopy allow us to obtain the torsional potential with high accuracy.

Due to steric and electronic interactions, the torsional potential of methyl groups attached to an aromatic compound are often hard to predict intuitively, while results from quantum chemical calculations are still rather not sufficiently accurate. Many investigations have been carried out on such aromatic systems, especially heterocyclic five-membered rings, to determine the methyl barrier heights, i.a. 2-methylthiazole (34.9 cm^{-1}) [1], 4-methylisothiazole (105.8 cm^{-1}) [2], 2,5-dimethylthiophene (248.0 cm^{-1}) [3], 2-acetyl-5-methylfuran (369.8 cm^{-1} for the *trans* conformer and 356.5 cm^{-1} for the *cis* conformer) [4], and 2,5-dimethylfuran (439.2 cm^{-1}) [5]. From those studies it is obvious that the torsional potentials of methyl groups attached to planar aromatic rings vary in a wide range in both, shape and height.

Pyrroles are nitrogen containing five-membered ring systems which possess unique organoleptic properties [6]. Some pyrroles are used as flavor additives. In the 1960s, pyrroles became known to represent a minor class of potentially significant flavor-associated compounds that occur naturally in foods. Pyrrole and the methyl substituted compound, 2-methylpyrrole (2MP), are found in volatile compounds from fried chicken [7]. Pyrrole also provides the key structural subunit for many of the most important biological molecules, such as heme and chlorophyll. Pyrrole and its derivatives exhibit wide range of biological and pharmaceutical activities, i.a. antibacterial, anti-fungal, anti-viral, anti-inflammatory, anti-cancer and antioxidant activity [8].

From a spectroscopic point of view, 2MP contains a methyl group which undergoes internal rotation and a ^{14}N nucleus which causes a nuclear quadrupole hyperfine structure. Within the scope of this work, a combination of quantum chemical calculations and MJ-FTMW spectroscopy was used to determine the shape of the potential function and the barrier to internal rotation. The quadrupole hyperfine structure yielded information on the electric field gradient at the site of the ^{14}N nucleus and consequently on the nature of its chemical bonds.

Quantum chemical calculations

To facilitate the spectral assignment, initial values of the rotational constants, the torsional potential, and the ^{14}N nuclear quadrupole coupling constants (NQCCs) were calculated by quantum chemical methods using the *GAUSSIAN16* program package [9].

Geometry optimizations

The molecular geometry of 2MP was optimized at different levels of theory with various combinations of the MP2, B3LYP, M06-2X, and CCSD methods with different basis sets to check for the convergence and to find out the level of theory which yields rotational constants in best agreement with the experimental values. A selection of the calculations is presented in Table 1. The predicted rotational constants are given along with the dipole moment components and the angle between the inertial principal *a* axis and the methyl rotor axis. For comparison, the experimental rotational constants are also shown. A full list with all calculations is given in Table S2 in the supplementary online material. The molecular geometry as optimized at the MP2/cc-pVDZ level of theory is shown in Figure 1.

Table 1. The rotational constants (in MHz), the angle between the inertial principal *a* axis and the internal rotor axis *i* (in degree), and the dipole moment components (in Debye) obtained by optimizations of the molecular geometry of 2MP at various levels of theory.

	A	*B*	*C*	∠(*i*,*a*)	$\|\mu_a\|$	$\|\mu_b\|$	$\|\mu_c\|$
MP2/6-311+G(d,p)	8536.0	3417.4	2478.4	2.82	1.16	1.72	0.00
MP2/6-311++G(d,p)	8533.9	3419.1	2479.1	2.80	1.16	1.71	0.00
B3LYP-D3/6-311+G(d,p)	8594.5	3427.0	2488.1	2.87	1.09	1.67	0.00
B3LYP-D3/6-311++G(d,p)	8595.3	3427.0	2488.1	2.86	1.09	1.66	0.00
MP2/cc-pVDZ	8462.7	3398.5	2462.7	2.75	1.07	1.79	0.00
MP2/cc-pVTZ	8607.6	3446.9	2499.5	2.77	1.08	1.73	0.00
B3LYP-D3/ cc-pVDZ	8535.3	3415.7	2477.7	2.80	1.03	1.79	0.00
B3LYP-D3/ cc-pVTZ	8639.7	3444.5	2500.9	2.84	1.02	1.69	0.00
CCSD/6-311++G(d,p)	8549.4	3413.6	2477.6	2.93	1.13	1.69	0.00
Experimental	8559.0	3432.5	2488.9	2.00			

It should be noted that the internal rotor axis is almost parallel to the principal *a* axis (see also the value of the angle $\angle(i,a)$ in Table 1). At equilibrium, the dihedral angle $\alpha = \angle(C_3,C_2,C_6,H_{11})$ is 0°, i.e. the methyl group is staggered with respect to the nitrogen atom.

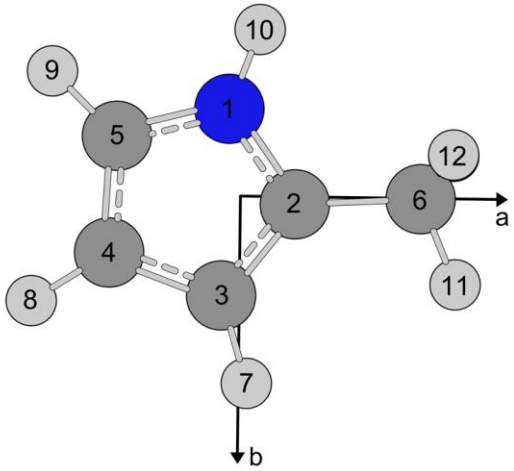


Figure 1. The molecular geometry of 2MP optimized at the MP2/cc-pVDZ level of theory. The atom numbering and the *a* and *b* inertial principal axis of inertia are given. The hydrogen atom H_{13} is located behind H_{12}.

Torsional potential of the methyl group

To obtain the barrier height to internal rotation and the shape of the potential function, geometry optimizations at the MP2/cc-pVDZ level of theory were carried out while the dihedral angle α was varied in steps of 10°. The resulting potential curve is given in Figure S1 in the supplementary online material. The potential was parameterized by a symmetry-adapted Fourier series with the Fourier coefficients given in Table S3 in the supplementary online material.

The torsional potential of 2MP displays the typical threefold shape caused by the symmetry of the methyl group. The potential consists of a V_3 value of 255.24 cm^{-1} with a V_6 contribution of 36.16 cm^{-1}.

^{14}N nuclear quadrupole coupling constants (NQCCs)

In many previous studies on nitrogen containing molecules [10, 11], the method of calculating ^{14}N NQCCs given by Bailey [12] turned out to be very reliable and was also applied in this work. At first, the molecular structure of 2MP was optimized at the MP2/cc-pVDZ level of theory. For this

optimized structure, the electric field gradient tensor of the ^{14}N nucleus in 2MP was computed at the B3PW91/6-311+G(d,p) level of theory, as recommended for π-conjugated system [13]. Using the calibration factor eQ/h = 4.599 MHz/a.u. [13], the quadrupole coupling tensor with the diagonal elements χ_{aa} = 1.331 MHz, χ_{bb} = 1.665 MHz, and χ_{cc} = –2.996 MHz, as well as the off-diagonal element χ_{ab} = 0.091 MHz was obtained. Due to the symmetry of the molecule χ_{ac} and χ_{bc} are zero.

Experiment

Measurements

2MP was purchased from abcr GmbH, Karlsruhe, Germany, with a stated purity of 95% and was used without further purification. A piece of pipe cleaner was soaked with the substance and inserted into a stainless steel tube placed upstream the nozzle. Helium, which was used as carrier gas, flowed over the substance at a pressure of 200-250 kPa.

All spectra were recorded using two MJ-FTMW spectrometers operating in the frequency ranges from 2.0 to 26.5 GHz [14] and from 26.5 to 40.0 GHz [15]. At first, a broadband scan was recorded from 12.0 to 14.9 GHz. The lines observed in the scan were remeasured at higher resolution. All lines show a hyperfine structure due to the nuclear quadrupole coupling of the ^{14}N nucleus. A typical spectrum is given in Figure 2.

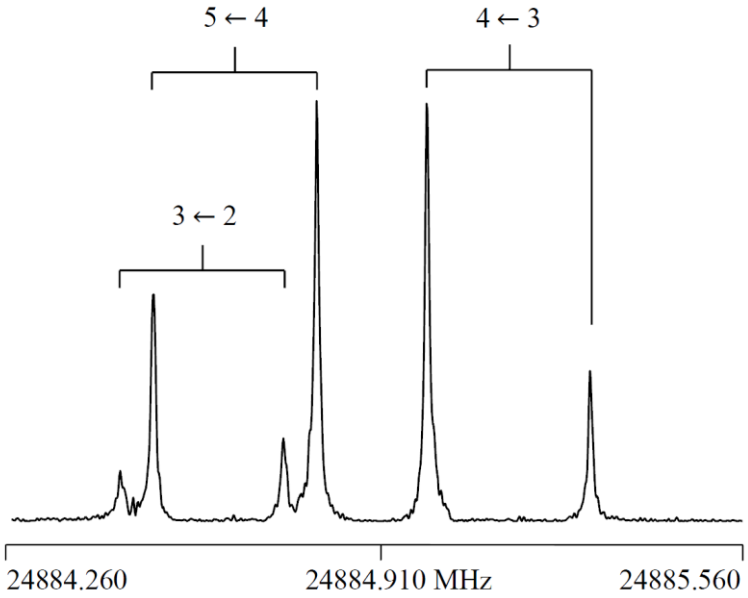


Figure 2. A high resolution spectrum of the $4_{14} \leftarrow 3_{03}$ A species transition of 2MP. The Doppler doublets are marked by brackets. The quantum numbers F' ← F are given at the respective

hyperfine component. For this spectrum, 153 free induction decays were co-added prior to Fourier transformation.

Spectral assignment

At the beginning of the assignment we predicted the spectrum with the *XIAM* code [16] using the rotational constants, the V_3 potential, and the angle between the internal rotor axis and the inertial *a* axis obtained by *ab initio* calculations at the MP2/cc-pVDZ level of theory, and neglected the quadrupole hyperfine splittings due to the ^{14}N nucleus. The predicted dipole moment components are $|\mu_a|$ = 1.07 D, $|\mu_b|$ = 1.79 D and $|\mu_c|$= 0.00 D (see Table 1). Therefore, A species *c*-type transitions were not expected to be observed in the spectrum. By comparing the broadband scan and the predicted spectrum the A and E torsional components of the $2_{11} \leftarrow 1_{10}$, $3_{03} \leftarrow 2_{12}$, $3_{21} \leftarrow 3_{12}$, and $4_{21} \leftarrow 4_{13}$ transitions could be identified. The linear combinations of the rotational constants $B_K = A - 0.5(B + C)$, $B_J = 0.5(B + C)$, $B_- = 0.5(B - C)$ and the V_3 potential were fitted, which enabled us to predict all other transitions with sufficient accuracy. Only one line in the scan region remained unassigned, which later turned out to be the *c*-type transition $1_{10} \leftarrow 0_{00}$ of the E species, which is nominally forbidden in the semi-rigid rotor approximation.

Afterwards, all lines were remeasured at high resolution. In this step, the quadrupole coupling effect was taken into account. The values of the NQCCs obtained by quantum chemical calculations were used to predict the hyperfine patterns, which fairly matched those of the experimental spectra. Due to spin-rotation and spin-spin interactions, some transitions show additional splittings of the order of 10 kHz. In those cases, the average of the individual components was taken.

Results and discussion

Results of the fits

Two global fits of 2MP with 62 A species and 67 E species lines with a total number of 359 hyperfine components were performed using the *XIAM* and *BELGI-C_s-hyperfine* [17] codes. The measurement accuracy is about 3.0 kHz for all lines. The root-mean-square (rms) deviations are 5.6 kHz and 3.1 kHz, respectively. The fit results are given in Table 2, the frequency list is available in Table S4 of the supplementary online material. The fit with *BELGI-C_s-hyperfine* was carried out in the rho axis system with the parameters defined in this coordinate system are given in Table 3.

For comparison with the *XIAM* results, some parameters were converted to the principal axis system (also presented in Table 2).

Table 2. Molecular parameters of 2MP in the inertial principal axis system obtained from fits with *XIAM* and *BELGI-C_s-hyperfine*.

Par.[a]	Unit	Fit *XIAM*	Fit *BELGI* [b]	*ab initio*[c]
A	MHz	8558.954(44)	8569.751(34)	8462.7
B	MHz	3432.5127(87	3432.832(38)	3398.5
C	MHz	2488.8717(87	2489.1935(69)	2462.7
Δ_J	kHz	0.2354(19)	0.2391 (11)	0.2236
Δ_{JK}	kHz	1.397(10)		1.4044
Δ_K	kHz	0.790(30)		0.5694
δ_J	kHz	0.06467(77)		0.0618
δ_K	kHz	0.401(18)		0.4222
F_o	GHz	158[d]		158.061
F	GHz	167.0422[e]	167.0422[f]	
V_3	cm^{-1}	279.7183(26)	278.9946(13)	255.24
ρ		0.0541[e]	0.0536021(93)	
D_{pi2J}	kHz	13.12(92)		
D_{pi2K}	MHz	1.1163(44)		
χ_{aa}	MHz	1.3345(20)	1.3342(11)	1.331
$\chi_{bb}-\chi_{cc}$	MHz	4.3599(36)	4.3600(33)	4.661
$\angle(i,a)$	°	2.002(46)	2.050(24)	2.75
$\angle(i,b)$	°	87.998(46)	87.950(24)	87.25
$\angle(i,c)$	°	90.0[g]	90.0[g]	90
rms[h]	kHz	5.6	3.1	
$N_A/N_E/Nq$[i]		62/67/359	62/67/359	

[a] All parameters refer to the inertial principal axis system. Statistical uncertainties are given as one standard uncertainty in the last digit. Watson's A reduction and I^r representation were used. [b] Obtained by transformation from the rho axis system to the principal axis system. [c] Calculated at the MP2/cc-pVDZ level. [d] Fixed to the calculated value. [e] Derived parameter. [f] Fixed to the value of Fit *XIAM*. [g] Fixed due to symmetry. [h] Root-mean-square deviation of the fit. [i] Number of A and E species transitions as well as number of the hyperfine components.

With the *XIAM* code, the three linear combination of rotational constants, five quartic centrifugal distortion constant Δ_J, Δ_{JK}, Δ_K, δ_J, δ_K, the ^{14}N NQCCs χ_{aa}, $\chi_{bb}-\chi_{cc}$, as well as the barrier to internal rotation V_3, the angle $\angle(i,a)$ between the *a* axis and the internal rotor axis and two higher order terms D_{pi2J}, D_{pi2K} enabled us to reproduce the experimental spectra to a *rms* deviation of 5.6 kHz.

In order to treat molecules containing one methyl rotor and one nitrogen nucleus, the *BELGI* code has been extended to its hyperfine versions *BELGI-C_s-hyperfine* and *BELGI-C_1-hyperfine*. Up to now, three molecular systems have been successfully treated by these codes, which are *N-tert*-butylacetamide (C_s) [17], *N*-ethylacetamide (C_1) [10] and 3-nitrotoluene (C_s) [18]. In this work, the *BELGI-C_s-hyperfine* code was applied, showing its capability to handle nuclear quadrupole coupling in the presence of internal rotation.

Table 3. Spectroscopic constants of 2MP in the rho axis system obtained using the program *BELGI-C_s-hyperfine*.

Par.[a]	Unit	Value	Operator
A	MHz	8568.696(23)	P_a^2
B	MHz	3433.887(29)	P_b^2
C	MHz	2489.1935(69)	P_c^2
D_{ab}	MHz	73.64(87)	$\{P_a,P_b\}$
Δ_J	kHz	0.2391 (11)	$-P^4$
Δ_K	kHz	0.736(17)	$-P_a^4$
Δ_{JK}	kHz	1.3174 (56)	$-P^2P_a^2$
δ_J	kHz	0.06585(43)	$-2P^2(P_a^2-P_c^2)$
δ_K	kHz	1.000(10)	$-\{P_a^2,(P_a^2-P_c^2)\}$
χ_{aa}	MHz	2.6683(22)	
χ_{bb}	MHz	3.0258(22)	
V_3	cm^{-1}	278.9946(13)	$(1/2)(1-\cos 3\alpha)$
ρ	unitless	0.0536021(93)	P_aP_α
F	cm^{-1}	5.57193[b]	$(P_\alpha-\rho P_a)^2$
F_v	MHz	-0.920(61)	$(1-\cos 3\alpha)P^2$
rms[c]	kHz	3.1	
$N_A/N_E/N_q$[d]		62/67/359	

[a] All parameters refer to the rho axis system and cannot be directly compared to those referring to the principal axis system. P_a, P_b, P_c are the components of the overall rotation angular momentum, P_α is the angular momentum conjugate to the internal rotation angle α. {u,v} is the anti-commutator uv + vu. The product of the parameter and operator from a given row yields the term actually used in the vibration-rotation-torsion Hamiltonian, except for F, ρ and A which occur in the Hamiltonian in the form $F(P_\alpha - \rho P_a)^2 + AP_a^2$, where $F = \hbar^2/2rI_\alpha$. Statistical uncertainties are shown as one standard uncertainty in the last digits. [b] Fixed to the value obtained from *XIAM* fit. [c] Root-mean-square deviation of the fit. [d] Number of A and E species transitions as well as hyperfine components. The nuclear quadrupole coupling constants are defined in the way that they are by a factor of two greater compared to their definitions in the *XIAM* program.

Discussion

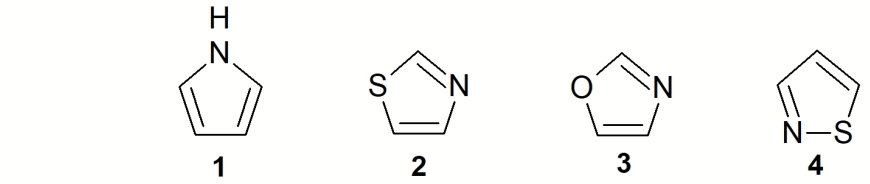
The rotational constants from the *XIAM* and the *BELGI-C_s-hyperfine* fits are in good agreement, however, they do not agree within their standard errors. This is due to the fact that different sets of parameters were used, and that the conversion of some RAM parameters to PAM parameters is not unique and introduces some errors. It turned out that the MP2 method as well as the DFT method with the B3LYP functional in combination with Grimme's dispersion correction and Becke-Johnson damping [19] yielded a good agreement with the experimental rotational constants for most sufficiently large basis sets. Rotational constants predicted with Truhlar's M06-2X method [20] are in general further off from the experimental values. Comparison between the rotational constants obtained from *XIAM* with those from *ab initio* calculations at the MP2/cc-pVDZ level of theory shows deviations of 1.12% for *A*, 0.99% for *B*, and 1.05% for *C* (with respect to the experimental values). A better agreement is not expected at the level of theory in use, because the experimental constants observed in the vibrational ground state are not directly comparable with the equilibrium values obtained from the *ab initio* calculations. From the results given in Table S2, the values of the rotational constants predicted at our most time-consuming calculations CCSD/6-311++G(d,p) are very close to the experimental values. Similar results can be achieved using a combination of the 6-31+G(d,p) or 6-31++G(d,p) basis set with the B3LYP or MP2 method, probably due to error compensation. From our experience, the same kind of error compensation always occurs at the same level of theory. Therefore, these levels might be chosen to predict reliable rotational constants to start the spectral assignment of future investigations on related methyl substituted pyrroles.

The parameters associated with the internal rotation, the V_3 potential and the angle between the principal *a* axis and the internal rotor axis $\angle(i,a)$, obtained from the *XIAM* and *BELGI* programs agree satisfactory, while the predicted V_3 potential is 8.8% lower than the experimental value. This deviation is rather large, however, it is in the expected range for quantum chemical calculations at the MP2/cc-pVDZ level of theory. In contrast to the geometry parameters, the calculations of the V_3 potential strongly depend on the method and basis set and a convergence is hard to achieve. Furthermore, the effects of zero point vibrations are known to influence the calculated value. Though the calculated potential also contains contributions of V_6 and higher order terms, they are assumed to be negligible in the potential function fitted with the current experimental data. With

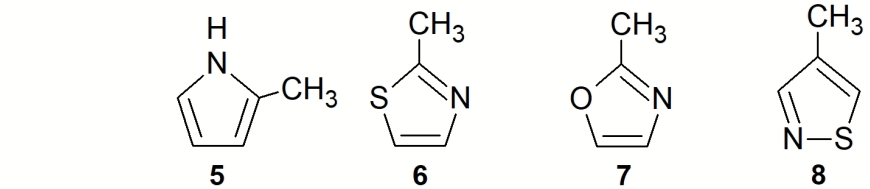
only transitions in the torsional ground state, it is impossible to test the validity of this assumption, as V_6 cannot be determined.

The ^{14}N NQCCs obtained from the *XIAM* and the *BELGI* fits agree within the standard errors. The quantum chemical results obtained at the B3PW91/6-311+G(d,p)//MP2/cc-pVDZ level agree within 0.3% for χ_{aa} and –6.9% for $\chi_{bb} - \chi_{cc}$ (with respect to the experimental values). In the principal axis system, an experimental value for χ_{ab} cannot be obtained because it is associated with the expectation value of $\{P_a,P_b\}$ which is zero in the case of the A species and which cannot be determined well from the E species at rather high barriers such as 280 cm^{-1} . If we calculate the same quantity in RAM and back-transform it to PAM, we will not be able to acquire χ_{ab}. Particularly in case of 2MP, the off-diagonal elements of the nuclear quadrupole coupling tensor could not be fitted with *BELGI-C_s-hyperfine* program and therefore a back-transformation on χ_{ab} was not possible.

Some results obtained for 2MP are compared with those of other five-membered heterocycles in Figure 3.



	1	**2**	**3**	**4**
Δ_c / uÅ^2	0.017	0.074	0.056	0.076
χ_{cc} / MHz	-2.704	2.41	2.663	1.37



	5	**6**	**7**	**8**
V_3 / cm^{-1}	280	34	252	106
Δ_c / uÅ^2	-3.223	-3.108	-3.127	-3.012
χ_{cc} / MHz	-2.846	2.390	2.117	1.459

Figure 3. Comparison of the V_3 potential, the inertial defect Δ_c, and the ^{14}N coupling constant χ_{cc} of 2MP with those of other five-membered heterocycles. (**1**) Pyrrole, (**2**) Thiazole, (**3**) Oxazole, (**4**) isothiazole, (**5**) 2-methylpyrrole, (**6**) 2-methylthiazole, (**7**) 2-methyloxazole, (8) 4-methylisothiazole.

The V_3 potential varies in a wide range from 34 cm^{-1} for 2-methylthiazole (**6**) [1], 106 cm^{-1} for 4-methylisothiazole (**8**) [2], 252 cm^{-1} for 2-methyloxazole (**7**) [21] to 280 cm^{-1} for 2MP (**5**). The V_3 potential is due to symmetry strictly 0 cm^{-1} for molecules with a C_{2v} symmetric frame and an internal rotor of C_{3v} symmetry. Only a small V_6 term is found in the cases of toluene [22], nitromethane [23, 24], and *N*-methylpyrrole [25]. If the frame symmetry is lowered from C_{2v} to C_s, then a V_3 contribution is observed, depending on the local asymmetry due to steric or electronic effects. In 2-methylthiazole (**6**) the nitrogen and sulfur atoms have similar effects on the methyl rotor and only a very low V_3 potential arises. In 4-methylisothiazole (**8**) a similar situation also leads to a rather low barrier of 106 cm^{-1}. In the title compound 2MP (**5**) the environment of the methyl group with a NH group on one side and a carbon atom on the other side is rather asymmetric which results in a much higher barrier. We note that such intuitive interpretations should be taken with caution because in aromatic systems electronic effects are easily propagated through the π system of the ring and affect the barrier height.

The aromaticity is associated with a planar structure of the π electron system. A direct measure for planarity is the inertial defect $\Delta_c = I_c - I_a - I_b$ with the principal moments of inertia I_a, I_b, I_c is calculated for all compounds in Figure 3. In the case of the non-methylated systems inertial defects of 0.017, 0.074, 0.056, and 0.076 u$Å^2$ are found for pyrrole (**1**) [26], thiazole (**2**) [27], oxazole (**3**) [28], and isothiazole (**4**) [29], respectively. The deviation from zero can be explained by the zero point vibrations of the rings. If one methyl group is attached to the ring, the out-of-plane hydrogen atoms of the methyl group cause an inertial defect close to 3.2 u$Å^2$. This is in agreement with the values of –3.223, –3.108, –3.127, and –3.012 u$Å^2$ of 2MP (**5**), 2-methylthiazole (**6**), 2-methyloxazole (**7**), and 4-methylisothiazole (**8**), respectively.

In all systems given in Figure 3 the principal *c* axis perpendicular to the ring plane is collinear with one principal axis of the coupling tensor. Therefore, the χ_{cc} element of the ^{14}N quadrupole coupling tensor can be directly compared. In pyrrole (**1)** and 2MP (**5**), the values of χ_{cc} are very similar but have a different sign than in all other heterocycles (**2-4)** and **(6-8**). The reason is, that the two groups exhibit a very different bond situation at the nitrogen atom which causes different electric field gradients at the site of the nitrogen nucleus. The electron configuration of nitrogen is $[He]2s^22p^3$. In all compounds of Figure 3, three sp^2 hybrid orbitals are formed, two of which are used to form the σ bonds to the neighboring atoms. One p orbital remains and becomes part of the π electron system. As shown in Figure 4, in the case of pyrrole three of five nitrogen

electrons are needed in three sp^2 orbitals to form the two N-C bonds and one N-H bond (not illustrated). The other two electrons occupy the p orbital (illustrated in red) and contribute to the π electron system. Altogether, there are 6 π electrons which, according to the 4n + 2 rule, makes pyrrole an aromatic compound.

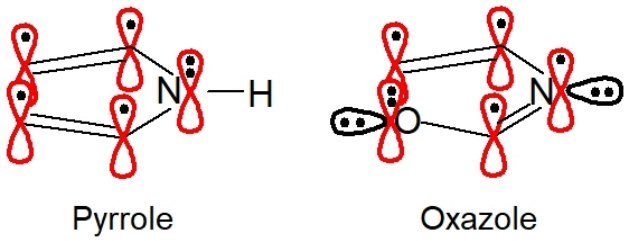


Figure 4. The π electron system in pyrrole and oxazole.

In the other heterocycles, the situation is quite different. For oxazole, two sp^2 orbitals of the nitrogen atom with one electron each form the bonds to the neighboring atoms (not illustrated). The third sp^2 orbital is occupied by an electron lone pair (illustrated in black). Only one electron remains in the p orbital (illustrated in red) contributing to the π electron system. It should be noted that in this group of molecules a sulfur or an oxygen atom is needed to donate two electrons for their p orbital to fulfill the condition for an aromatic compound (6 electrons in the π system). Similar considerations apply also to thiazole and isothiazole.

In the case of pyrrole, the effect of methylation on χ_{cc} is small. Despite the well-known +I effect [30] of methyl groups, only a small change in the field gradient tensor is observed. The values of χ_{cc} of pyrrole (**1**) and 2MP (**5**) are -2.704 and -2.846 MHz, respectively. Similar small effects are observed upon methylation of thiazole (**4**), oxazole (**6**), and isothiazole (**8**).

Conclusion

The methyl torsional fine structure and the quadrupole hyperfine structure in the rotational spectrum of 2MP could be fully resolved using two molecular jet Fourier transform microwave spectrometers operating in the frequency range from 2 to 40 GHz. All observed transitions were analyzed and fitted with the programs *XIAM* and *BELGI-C_s-hyperfine*, whereby the *BELGI-C_s-hyperfine* code enabled us to reproduce the whole data set close to measurement accuracy. The spectroscopic work was supplemented by quantum chemical calculations.

The methyl group undergoes internal rotation with a V_3 hindering potential of 279.7183(26) cm^{-1}. The quadrupole coupling constants of the ^{14}N nucleus were determined with very high accuracy. Calculations of the electric field gradient tensor with Bailey's method yielded nuclear coupling constants in good agreement with the experimental values.

Disclosure statement

No potential conflict of interest was reported by the authors.

Funding

T. N. thanks the Doctoral School of Environmental Science of Île-de-France (DS 129) for a Ph.D grant. Simulations were performed with computing resources granted by RWTH Aachen University under project rwth0369. W.S. thanks the Université Paris-Est for an invited researcher grant which enabled him to work at the Université Paris-Est Créteil. This work was supported by the Agence Nationale de la Recherche ANR (project ID ANR-18-CE29-0011).

Acknowledgement

I.K., H.V.L.N., and T.N. thank the DIM Qi2 for supporting the organization of the Journées de Spectroscopie Moléculaire (JSM) in Créteil where T.N. presented a poster with the results. C.D. thanks the DIM Qi2 for supporting her trip to the JSM.

References

[1] J.-U. Grabow, H. Hartwig, N. Heineking, W. Jäger, H. Mäder, H.W. Nicolaisen, W. Stahl, J. Mol. Struct. **612**, 349 (2002).

[2] H.W. Nicolaisen, J.-U. Grabow, N. Heineking, W. Stahl, Z. Naturforsch. **46a**, 635 (1991).

[3] V. Van, W. Stahl, H.V.L. Nguyen, Phys. Chem. Chem. Phys, **17**, 32111 (2015).

[4] V. Van, W. Stahl, H.V.L. Nguyen, ChemPhysChem **17**, 3223 (2016).

[5] V. Van, J. Bruckhuisen, W. Stahl, V. Ilyushin, H.V.L. Nguyen, J. Mol. Spectrosc. **343**, 121 (2017).

[6] J.A. Maga, J. Agric. Food Chem. **29**, 691 (1981).

[7] J. Tang, Q.Z. Jin, G.-H. Shen, C.T. Ho, S.S. Chang, J. Agric. Food Chem. **31**, 1287 (1983).

[8] R. Kaur, V. Rani, V. Abbot, Y. Kapoor, D. Konar, K. Kumar, J. Pharm. Chem. Chem. Sci. **1**, 17 (2017).

[9] M.J. Frisch, G.W. Trucks, H.B. Schlegel, G.E. Scuseria, M.A. Robb, J.R. Cheeseman, G. Scalmani, V. Barone, G.A. Petersson, H. Nakatsuji, X. Li, M. Caricato, A.V. Marenich, J. Bloino, B.G. Janesko, R. Gomperts, B. Mennucci, H.P. Hratchian, J.V. Ortiz, A.F. Izmaylov, J.L. Sonnenberg, D. Williams-Young, F. Ding, F. Lipparini, F. Egidi, J. Goings, B. Peng, A. Petrone, T. Henderson, D. Ranasinghe, V.G. Zakrzewski, J. Gao, N. Rega, G. Zheng, W. Liang, M. Hada, M. Ehara, K. Toyota, R. Fukuda, J. Hasegawa, M. Ishida, T. Nakajima, Y. Honda, O. Kitao, H. Nakai, T. Vreven, K. Throssell, J.A. Montgomery, Jr., J.E. Peralta, F. Ogliaro, M.J. Bearpark, J.J. Heyd, E.N. Brothers, K.N. Kudin, V.N. Staroverov, T.A. Keith, R. Kobayashi, J. Normand, K. Raghavachari, A.P. Rendell, J.C. Burant, S.S. Iyengar, J. Tomasi, M. Cossi, J.M. Millam, M. Klene, C. Adamo, R. Cammi, J.W. Ochterski, R.L. Martin, K. Morokuma, O. Farkas, J.B. Foresman, D.J. Fox, *Gaussian 16*, Revision B.01, Gaussian, Inc., Wallingford CT, 2016.

[10] R. Kannengießer, M.J. Lach, W. Stahl, H.V.L. Nguyen, ChemPhysChem. **16**, 1906 (2015).

[11] R. Kannengießer, S. Klahm, H.V.L. Nguyen, A. Lüchow, W. Stahl, J. Chem. Phys. **141**, 204308 (2014).

[12] W.C. Bailey, Chem. Phys. **252**, 57 (2000).

[13] R. Kannengießer, W. Stahl, H.V.L. Nguyen, W.C. Bailey, *J. Mol. Spectrosc.* **317**, 50 (2015).

[14] J.-U. Grabow, W. Stahl, H. Dreizler, Rev. Sci. Instrum. **67**, 4072 (1996).

[15] I. Merke, W. Stahl, H. Dreizler, Z. Naturforsch. **49a**, 490 (1994).

[16] H. Hartwig, H. Dreizler, *Z. Naturforsch*. **51a**, 923 (1996).

[17] R. Kannengießer, W. Stahl, H.V.L. Nguyen, I. Kleiner, J. Phys. Chem. A **120**, 3992 (2016).

[18] A. Roucou, I. Kleiner, M. Goubet, S. Bteich, G. Mouret, R. Bocquet, F. Hindle, W.L. Meerts, A. Cuisset, ChemPhysChem. **19**, 1056 (2018).

[19] E. Caldeweyher, C. Bannwarth, S. Grimme, J. Chem. Phys. **147**, 034112 (2017).

[20] Y. Zhao, D.G. Truhlar, Theor. Chem. Acc. **120**, 215 (2008).

[21] E.R.L. Fliege, Z. Naturforsch. **45a**, 911 (1990).

[22] V. V. Ilyushin, E. A. Alekseev, Z. Kisiel , L. Pszczółkowski, J. Mol. Spectrosc. **339**, 31 (2017).

[23] F. Rohart, J. Mol. Spectrosc. **57**, 301 (1975).

[24] V. V. Ilyushin, J. Mol. Spectrosc. **345**, 64 (2018).

[25] J. Makarewicz, S. Huber, B. Brupbacher-Gatehouse, A. Bauder, J. Mol. Struct, **612**, 117 (2002).

[26] L. Nygaard, J.T. Nielsen, J. Kirchheiner, G. Maltesen. J.R. Andersen, G.O. Sørensen, J. Mol. Struct. **3**, 491 (1969).

[27] L. Nygaard, E. Asmussen, J.H. Høg, R. C. Maheshwari, C.H. Nielsen, I.B. Petersen, J. Rastrup-Andersen, G.O. Sørensen, J. Mol. Struct. **8**, 225 (1971).

[28] A. Kumar, J. Sheridan, O.L. Stiefvater, Z. Naturforsch. **33a**, 145 (1978).

[20] J.H. Griffiths, A. Wardley, V.E. Williams, N.L. Owen, J. Sheridan, Nature **216**, 1301 (1967).

[30] C.K. Ingold, J. Chem. Soc. 1120 (1933).